Draft Version February 19, 2022
Preprint typeset using LaTeX style emulateapj v. 5/2/11

CHARACTERIZING THE GALACTIC WHITE DWARF BINARY POPULATION WITH SPARSELY SAMPLED RADIAL VELOCITY DATA

Dan Maoz [1], Carles Badenes[2,1,3], Steven J. Bickerton [4]

Draft Version February 19, 2022

ABSTRACT

We present a method to characterize statistically the parameters of a detached binary sample – binary fraction, separation distribution, and mass ratio distribution – using noisy radial-velocity data with as few as two, randomly spaced, epochs per object. To do this, we analyze the distribution of $\Delta\mathrm{RV_{max}}$, the maximum radial-velocity difference between any two epochs for the same object. At low values, the core of this distribution is dominated by measurement errors, but for large enough samples there is a high-velocity tail that can effectively constrain the parameters of the binary population. We discuss our approach for the case of a population of detached white-dwarf (WD) binaries with separations that are decaying via gravitational wave emission. We derive analytic expressions for the present-day distribution of separations, integrated over the star-formation history of the Galaxy, for parametrized initial WD separation distributions at the end of the common-envelope phase. We use Monte Carlo techniques to produce grids of simulated $\Delta\mathrm{RV_{max}}$ distributions with specific binary population parameters, and the same sampling cadences and radial velocity errors as the observations, and we compare them to the real $\Delta\mathrm{RV_{max}}$ distribution to constrain the properties of the binary population. We illustrate the sensitivity of the method to both the model and observational parameters. In the particular case of binary white dwarfs, every model population predicts a merger rate per star which can easily be compared to specific type-Ia supernova rates. In a companion paper, we apply the method to a sample of ~ 4000 WDs from the Sloan Digital Sky Survey. The binary fractions and separation distribution parameters allowed by the data indicate a rate of WD-WD mergers per unit stellar mass in the Galactic disk, $\sim 1\times10^{-13}$ mergers $\mathrm{yr^{-1}\,M_\odot^{-1}}$, remarkably similar to the rate per unit mass of Type-Ia supernovae in Milky-Way-like galaxies.

Subject headings: binaries:close, spectroscopic — white dwarfs — supernovae: general

1. INTRODUCTION

Stellar multiplicity is a fundamental piece in our current picture of stellar formation and evolution. Modern studies of stellar multiplicity aim to constrain the fraction of stars with companions (or multiplicity fraction, f_m), the distribution of separations, and the dependence of these parameters on variables like stellar mass, age, and metallicity. Different observational techniques are used to probe different separation and flux contrast regimes (Duquennoy & Mayor 1991; Makarov & Kaplan 2005; Mason et al. 2009; Metchev & Hillenbrand 2009; Raghavan et al. 2010). Short-period binary systems are of particular interest as the ancestors of future interacting binaries, from cataclysmic variables to novae, high and low-mass X-ray binaries, supersoft X-ray sources, and Type Ia supernovae. However, the fundamental properties of short-period binaries in the Galaxy are still poorly constrained. This has important implications for testing specific scenarios for the formation of multiple stellar systems (Tohline 2002; Goodwin & Kroupa 2005; Bressert et al. 2010; Marks et al. 2011), stellar population synthesis models (Bruzual & Charlot 1993; Conroy et al. 2009; Marks & Kroupa 2011), and birth rate calculations for their interacting descendants (Belczynski & Taam 2004; Ruiter et al. 2009).

The first modern spectroscopic survey for close stellar binaries was performed by Duquennoy & Mayor (1991), who examined 164 F and G-type stars, taking more than 4200 individual radial velocity (RV) measurements. Such surveys are extremely labor intensive, because they need to obtain enough RV measurements of each target to either confidently discard multiplicity up to a certain period threshold, or to derive an orbital solution of sufficient quality. For example, the recent study by Raghavan et al. (2010) examined 454 solar-type stars with different techniques (including RVs), only a factor 3 improvement over Duquennoy & Mayor (1991) in almost twenty years. The advent of large spectroscopic data bases like the Sloan Digital Sky Survey (SDSS, York et al. 2000) opens the possibility to take RV surveys to the next level, allowing millions of RV measurements of hundreds of thousands of different stars with well-calibrated and stable instrumental set-ups.

In this paper, we present a method to characterize binary populations statistically based on large samples of noisy RVs, with only a few epochs per target, but without followup observations, confirmations of real binaries, and derivations of orbital parameters for individual systems. The observable that we analyze is the distribution of maximum RV differences, $\Delta\mathrm{RV_{max}}$, which is straight-

[1] School of Physics and Astronomy, Tel-Aviv University, Tel-Aviv 69978, Israel; maoz@astro.tau.ac.il
[2] Department of Physics and Astronomy and Pittsburgh Particle Physics, Astrophysics, and Cosmology Center (PITT-PACC), University of Pittsburgh, 3941 O'Hara Street, Pittsburgh, PA 15260, USA; badenes@pitt.edu
[3] Benoziyo Center for Astrophysics, Weizmann Institute of Science, Rehovot 76100, Israel
[4] Department of Astrophysical Sciences, Princeton University, Peyton Hall, Ivy Lane, Princeton, NJ 08544-1001, USA; bick@astro.princeton.edu

forward to obtain from a set of RV measurements for a sample of stars. This distribution contains information about the orbital velocity amplitudes of some members of some of the close binaries in a sample of stars. The use of velocity differences assures that the (uninteresting in the present context) systemic velocities of the stars are subtracted out of the dataset, along with any other time-constant velocity offsets (wavelength calibration errors, gravitational redshifts, etc.). Naturally, the more times a system is observed, the higher the chances of catching its full orbital RV variation amplitude, but even with only two epochs per system, some fraction of that amplitude will be probed. Apart from the observed RVs themselves and their sampling times, accurate knowledge of the distribution of RV measurement errors is essential. We illustrate how the sensitivity of the method depends on these observational characteristics.

Tutukov & Yungelson (1986) outlined such an approach schematically, as a way to discover close binary white dwarfs (WDs). The first application of this kind of technique (though in a more rudimentary way) was by Maxted & Jeffries (2005). A slightly different approach that has been applied to SDSS data is described in Clark et al. (2011). Here, we present the method in the context of the problem of characterizing a population of detached WD binaries whose separations are decaying via gravitational wave emission. In a companion paper (Badenes & Maoz 2012; Paper II), we apply the method to a sample of ~ 4000 WDs from the SDSS with multiple-epoch spectra, we constrain the sample's binary population parameters, and we estimate its gravitational-wave-driven merger rate.

2. MONTE CARLO SIMULATION OF THE ΔRV_{max} DISTRIBUTION OF A BINARY POPULATION

We now simulate the ΔRV_{max} distribution of an assumed binary population. Our methodology can be applied to any binary population, but we will focus here on detached binary WDs in the Galactic disk, with the aim, in Paper II, of finding the regions of parameter space that describe a binary population that are allowed by the observed ΔRV_{max} distribution for a sample of SDSS WDs. We simulate WD binaries with properties drawn, in a Monte-Carlo process, from possible families of distributions of these properties, as detailed below. We then "observe" the simulated systems with the sampling sequences and the velocity error distributions of the real data, to produce each model ΔRV_{max} distribution. A detached WD binary will merge, due to loss of energy and angular momentum to gravitational wave emission, within a time dictated by its separation and its component masses. A corollary of every population model will therefore be a prediction of the model's WD merger rate (whether sub-Chandrasekhar or super-Chandrasekhar), which can be directly compared to observed type-Ia supernova rates, or to the rates of other transient events that are candidates for the outcomes of such mergers. We describe below each step in this modeling process.

Our modeling approach is distinct from that of "binary population synthesis" (BPS) calculations such as Toonen et al. (2011), Mennekens et al. (2010), Wang et al. (2010), or Ruiter et al. (2009). In BPS, one begins by simulating a population of main-sequence binaries, with a chosen mass and separation distribution, and one then attempts to follow the complex stages of stellar and binary evolution of each system, including mass transfer, mass loss, common envelope evolution, and so on. BPS calculations have many free parameters. Apart from the parameters that specify the initial conditions, there is a variety of parametrized ways to approximate the physics of various stages of evolution, particularly the common-envelope phases. Because of this variety and freedom, there is a great range among the predictions of different BPS calculations for the characteristics of the final WD populations. Instead, our approach is to parametrize in a simple mathematical way the properties of the binary population at the *end* of its complex physical evolution – for binary WDs, at the end of the last common-envelope phase. Beyond that phase, there is only well-understood and easily modeled orbit decay due to gravitational wave emission. The general forms of our parametrizations for the component masses and separations at this evolved stage are guided by direct observations, by BPS results, or by educated guesses. They are thus more realistic than those based solely on a particular BPS realization, but they also allow investigating a larger parameter space for what the binary population might actually be like. The real RV measurements can then select the particular allowed regions of this parameter space.

2.1. *WD primary mass*

For every simulated WD system (either single or binary) we begin by assigning a primary mass ('primary' and 'secondary' refers here to the larger and smaller mass, respectively, not to which star will dominate the spectral energy distribution). We draw the primary mass, m_1, from the observed distribution of WD masses determined by Kepler et al. (2007) for 1859 hot (effective temperature $T_{\rm eff} > 12000$ K) and bright ($g \leq 19$ mag) DA WDs in the DR4 SDSS catalog. We do not use the mass functions implied for the cooler WDs in each class, as Kepler et al. (2007) point out and discuss the uncertainty in the atmospheric modeling of those cool WD, which likely leads to a systematic over-estimate of their masses. The mass distribution is composed of four Gaussian components – a main, narrow, component centered at 0.58 $M_\odot$ with 1σ width of 0.047 $M_\odot$, and three weaker components centered at lower and higher masses. The latest version of the SDSS WD catalog, corresponding to DR7, has over 17000 entries (Kleinman et al. 2009)[5]. The Kepler et al. (2007) sample is a subset of the DR7 WD sample that we actually analyze in Paper II, and so its mass distribution is likely quite representative of that of the WDs that we see in our sample. As a consistency check, we have measured the mass distribution for hot and bright DA WDs in the DR7 catalog, using the $T_{\rm eff}$ and effective gravity, $\log g$, values fitted by Kleinman et al., and the cooling curves of Fontaine et al. (2001) [6]. We have confirmed with a KS test that this distribution is very close to the one obtained by Kepler et al. for the DR4 WDs.

[5] The catalog has not been published yet, but it was kindly made available to us by S. Kleinman (private communication). The version that we use here is from July 2010, and it has 17371 entries.

[6] We obtained an updated version of these cooling curves from `http://www.astro.umontreal.ca/~bergeron/CoolingModels/`.

It is likely that, contrary to our assumption above, WD primaries do not have the same mass distribution as single WDs. Mass transfer and mass loss in close binaries can lead to either an increase or a decrease in the primary WD's final mass. In the BPS calculations of Claeys et al. (2011), based on the code of Izzard et al. (2006), the primaries in WD pairs with separations of $< 14R_{\odot}$ have a broad mass distribution, between 0.3 and 0.9 $M_{\odot}$ (J. Claeys 2011, private communication). However, we find that even rather drastic changes in the primary mass function have only a small effect of the ΔRV_{max} distribution and on the merger rate. We have changed the center of the main Gaussian mass component to as low as 0.4 $M_{\odot}$ or as high as 0.8 $M_{\odot}$, and find a negligible effect of the ΔRV_{max} distribution. Increasing the 1σ width to 0.2 $M_{\odot}$ also has only a small effect on ΔRV_{max} (at the level of, e.g., increasing the distribution by $\sim 20\%$ at ΔRV_{max}=300km s^{-1}; see below). Our conclusions will therefore not depend on the particular form we have assumed for the WD primary mass distribution. The weak dependence of ΔRV_{max}, in general, on the details of the binary mass components, is discussed further in Section 3.

2.2. *Binary fraction*

One major binary population parameter to be constrained by data is the fraction of objects of a class that is in binary systems. As we will see below, an analysis of a ΔRV_{max} distribution can be sensitive only to binary systems with velocities in the tail of the distribution, beyond a "core" that is dominated by single systems and random velocity errors. For example, for the SDSS WD sample analyzed in Paper II, this threshold is at ΔRV_{max} $\gtrsim$250 km s^{-1}. For the range of possible binary component masses in a population, this velocity-difference threshold effectively puts an upper limit on the binary separations that can be probed. In an extreme-mass-ratio WD binary with masses $m_1 = 1.2\,M_{\odot}$ and $m_2 = 0.2$ $M_{\odot}$, the secondary (m_2) will achieve such orbital peak-to-trough velocity amplitude if the separation is $\lesssim$0.05 AU. For individual WDs with low-noise measurements and long temporal baselines, the SDSS data might be able to detect binaries with larger separations, but our analysis does not single out such systems. Therefore, we will define the binary population parameter, f_{bin}, as the fraction of all WD systems (both single systems and binary systems) that are binary systems with separations $a < 0.05$ AU. The length of an individual exposure determines the minimum separation that we can detect. For the SDSS sample, the individual exposure times are $\sim$15 min. For the lowest WD masses, $\sim$ 0.2 $M_{\odot}$, this corresponds to separations of $\sim 10^5$ km, or only about 10 WD radii. Thus, the SDSS data can probe binary separations ranging from close to Roche-lobe overflow, and out to 0.05 AU, which corresponds to periods of about 4 days for typical WD masses. Since all double-degenerate (DD) systems that merge within a Hubble time have periods shorter than $\sim$ 12 hours, this is more than adequate to provide an estimate of the local WD merger rate.

However, the binary fraction cannot be considered independent of the masses of the WD components. From the initial-final mass relation for stars and WDs (e.g. Williams et al. 2009), it is known that WDs with masses less than $m_{lim} \approx 0.45$ $M_{\odot}$ have not had enough time to form in isolation over the age of the Universe, and therefore such WDs must be in binaries, with separations that permit interactions in the course of the stellar evolution of the components. This was first shown directly by Marsh et al. (1995), who found that five out of the seven WDs that they studied, with masses below 0.45 $M_{\odot}$ had WD companions with periods $P < 5$ d. Rebassa-Mansergas et al. (2011) have shown that, in binaries composed of a main-sequence star and a WD of mass $\lesssim$ 0.5 $M_{\odot}$, the period is generally $\lesssim$ a few days. Most recently, Brown et al. (2012) mined the SDSS photometrically for WDs with masses < 0.25 $M_{\odot}$. After follow-up spectroscopy, they found that such low-mass WDs are always, or almost always, in close binaries, with periods of less than 1 day, and often with a relatively massive WD (or possibly neutron star) companion. The extremely low-mass WDs actually found and followed up by Brown et al. (2012) turn out to have even lower masses, always < 0.20 $M_{\odot}$. It is not known at what precise mass the *close* ($P \lesssim 1$ d) binary fraction becomes 100%.

To account for this effect, we adopt a limit $m_{lim} = 0.25$ $M_{\odot}$, such that when our simulated primary WD mass is smaller than m_{lim}, we always assign it to be in a binary. The fraction of the Kepler et al. mass function that is below this mass means that, effectively, we assign 0.07% of the WDs in the simulated sample to be in binaries in which one of the WDs is less massive than 0.25 $M_{\odot}$. Naturally, close companions likely exist also around all WDs with somewhat higher masses, e.g., < 0.35 $M_{\odot}$ (which constitute 2.5% of the Kepler et al. 2007 WDs) or < 0.45 $M_{\odot}$ (9%). However, we do not know for a fact, for those higher masses, that the orbits are within the 0.05 AU limit that we have set above, when defining close binarity. Indeed, the high-ΔRV_{max} tail of our observed sample in Paper II is *not* dominated by low-mass objects, but rather by typical, ~ 0.6 $M_{\odot}$, WDs, as shown in Fig.1. Thus, f_{bin} in our simulations is the fraction of systems with separations $a < 0.05$ AU, and with both components with masses above $m_{lim} = 0.25$ $M_{\odot}$. Every simulation includes an additional population of extremely-low-mass ($m < m_{lim}$) WDs that are all in binaries and are not counted in f_{bin}. To investigate how our results depend on the choice of m_{lim}, we have also calculated models with $m_{lim} = 0.35$ $M_{\odot}$ and 0.45$M_{\odot}$. As was the case, above, with variations in the primary WD mass function, we find only weak effects on the ΔRV_{max} distribution, as long as the total fraction of binaries is equal (e.g., a model with $m_{lim} = 0.25$ $M_{\odot}$ and f_{bin}=0.05 gives a very similar ΔRV_{max} distribution as a model with $m_{lim} = 0.35$ $M_{\odot}$ and f_{bin}=0.025, for which the total binary fraction (including systems with a WD of mass $< m_{lim}$) equals 0.05. Thus, our conclusions will not depend on the exact choice of m_{lim}.

For the fraction f_{bin} of the simulated WDs, as well as the extremely-low-mass WD binaries, we assign additional binary parameters, as described below. To the remaining $1-f_{bin}$ WDs, we assign an orbital velocity of zero, and skip directly to the allocation of random velocity errors at several observing epochs (Section 2.6). The maximum difference between these random errors for each such non-close-binary WD will then constitute the simulated ΔRV_{max} for that WD.

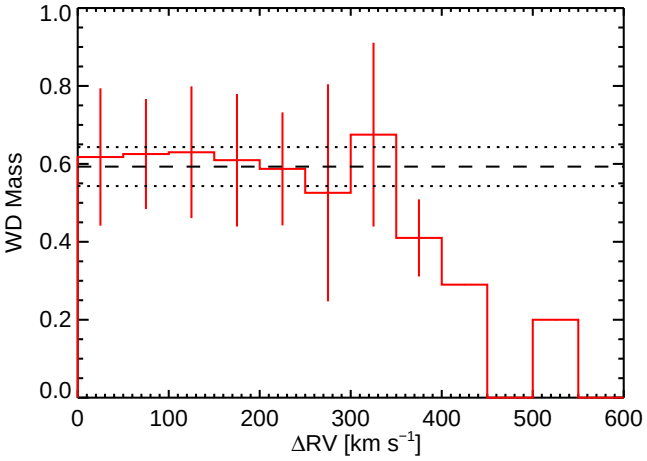

FIG. 1.— Mean and rms (shown with error bars) masses of the photometric primaries in the observed sample of Paper II, based on spectral modeling of the WDs, for various bins of ΔRV_{max}. The WDs with large $\Delta RV_{max}(> 200$ km s$^{-1})$ which reflect the close binaries in the sample, have masses ~ 0.6 M$_\odot$, similar to single WDs, whose mean and rms mass range is shown by the horizontal dashed and dotted lines. The bins without error bars are based on only one system each, and the 375 km s^{-1} bin is based on two systems.

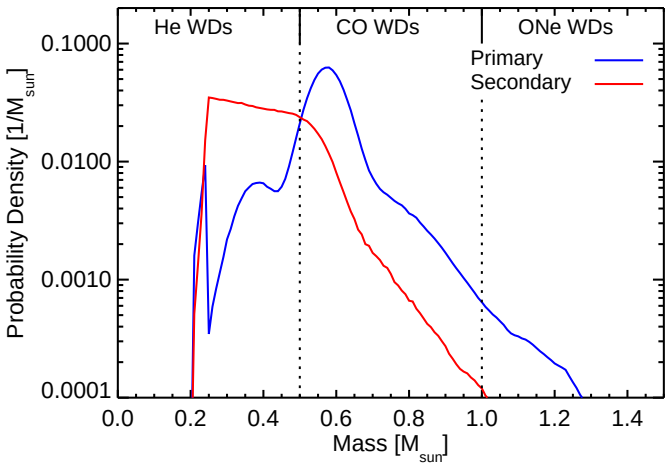

FIG. 2.— Probability density distribution of primary (blue) and secondary (red) masses in our model binary WD population. A binary fraction of f_{bin}=0.05 is assumed in this example, and this sets the height of the extremely low-mass WD peak (< 0.25 M$_\odot$), in which WDs are always in close binaries. A flat mass-ratio distribution ($\beta = 0$) is also assumed in this example. We note that the two distributions are not independent. For illustration, the theoretical boundaries between He, CO, and ONe WDs in isolated stars are shown with vertical lines.

2.3. *WD secondary mass*

The mass of the secondary, m_2, is not likely to be drawn from the same distribution as m_1. Already in main-sequence binaries, it is clear that the secondary mass is not drawn from the initial mass function, but rather from a mass-ratio distribution that is approximately flat (Raghavan et al. 2010). However, there is little in the way of observational or theoretical guidance for choosing the mass distribution of post-common-envelope WD secondaries. Of the ∼40 known DD systems, only 10 are double-lined, i.e., with detected spectral features from both components. For these systems, both WD masses can be determined, but the number is still too small to say much about the mass distribution. In the BPS calculations of Claeys et al. (2011) the secondary WDs have a roughly flat mass-ratio distribution. We therefore choose the following parametrization. In cases where m_1 is above m_{lim}, if the simulated system is a binary, we draw the secondary WD mass from a power-law distribution in mass ratio,

$$P(q) \propto q^\beta, \qquad q \equiv m_2/m_1, \tag{1}$$

with m_2 between m_{lim} and m_1. The power-law index β is one of the parameters that we vary among the realizations of our simulation, in order to constrain the properties of the WD binary population. In cases where the primary in the Monte-Carlo draw was below m_{lim} (and therefore the star is always in a binary), the second star is chosen with equal probability between 0.2 M$_\odot$ and 1.2 M$_\odot$. In this scheme, since the typical mass primary has a mass ~ 0.6 M$_\odot$, the secondary will have, on average, a mass of ~ 0.4 M$_\odot$, reflecting the observed commonness of low-mass WDs in close binaries (e.g. Rebassa-Mansergas et al. 2011).

For illustration purposes, we have plotted these primary and secondary mass distributions in Figure 2, with $\beta = 0$. We have overlaid the standard boundaries between He, CO, and ONe cores in isolated WDs (0.5 and 1.0 M$_\odot$, respectively), but we note that these boundaries might not apply to close binary systems (see Prada Moroni & Straniero 2009).

2.4. *Separation distribution*

Next, we assign to each simulated DD system a separation, and hence we need to consider what are the possible separation distributions for close binary WDs. The separation distribution at the time the WDs emerge from their final common envelope phase is unknown observationally, while theoretically it is a longstanding, complex, and unsolved problem (see Ivanova 2011, for a recent review). The close WDs may undergo either one or two common-envelope phases (Woods et al. 2012), which could, in principle, lead to a complicated separation distribution. Nevertheless, BPS calculations, as well as some more sophisticated treatments (Deloye & Taam 2010), suggest a power-law separation distribution with a negative index, over the range of separations that we consider here, $\sim 0.1 - 10$ R$_\odot$. In the BPS calculations of Claeys et al. (2011), over the range of separations that we consider, the post-common-envelope initial WD separations indeed are roughly constant per logarithmic interval (J. Claeys, private communication). The same is true in the BPS models of Yungelson (2010), at least for separations above ~ 1 R$_\odot$ (L. Yungelson, private communication). The $\sim t^{-1}$ Type-Ia supernova delay-time distributions generally predicted by BPS models for the DD channel would not arise if the WD initial separation distributions were not approximately of the above form (see, e.g. Maoz & Mannucci 2011).

Therefore, we will assume an initial WD separation distribution that is a power law, with an index that is a free parameter to be constrained by observations. Whatever the initial distribution, orbital decay due to gravitational wave emission will immediately begin to modify it, as all of the orbits shrink and the innermost systems merge. Furthermore, the actual distribution at any particular time will be the sum of the distributions of many populations of different ages, that have evolved over dif-

ferent amounts of time. We now calculate the form of this eveolved, time-integrated, distribution.

2.4.1. *Evolution of a binary separation distribution due to gravitational wave losses*

The separation a of two point masses, m_1 and m_2, in a circular-orbit binary, will shrink over time due to gravitational wave energy loss as

$$\frac{da}{dt} = -\frac{K}{4a^3}, \qquad K \equiv \frac{256}{5}\frac{G^3}{c^5} m_1 m_2 (m_1 + m_2), \tag{2}$$

where G is the gravitational constant and c is the speed of light (Peters & Mathews 1963). From integration, the time t for the system to evolve from separation a' to separation a obeys

$$a'^4 - a^4 = Kt. \tag{3}$$

Suppose a population of WD binaries is formed at a time $t = 0$ (this could be, e.g., a population of WD binaries in the Galaxy that have just emerged from the common envelope phase). The population has an initial distribution of separations $n'(a')$. For simplicity, we will assume the initial distribution of WD masses is independent of separation. Systems with separations in the range a' to $a' + da'$ will migrate, after a time t, to a bin a to $a + da$ in the evolved distribution $n(a, t)$. Conservation of the number of systems (except for those systems that reach $a = 0$ and merge) requires that

$$n(a, t)da = n'(a')da', \tag{4}$$

or

$$n(a,t) = n'(a')\frac{da'}{da} = n'(a')\left(\frac{a}{a'}\right)^3 \tag{5}$$

$$= n'[(a^4 + Kt)^{1/4}]\frac{a^3}{(a^4 + Kt)^{3/4}}.$$

If the initial distribution is a power law,

$$n'(a') \propto a'^{\alpha}, \tag{6}$$

then

$$n(a, t) \propto a^3(a^4 + Kt)^{(\alpha-3)/4}. \tag{7}$$

The evolved distribution at time t is thus approximately a broken power law. For separations $a \gg (Kt)^{1/4}$ (i.e., much larger than those that can merge within time t), the distribution will have approximately the original power-law slope, $n(a) \sim a^{\alpha}$. At separations $a \ll (Kt)^{1/4}$, on the other hand, $n(a) \sim a^3$ (see left panel of Figure 3). The merger rate versus time from this single-age population will be controlled by the short separation pairs for which $a \ll (Kt)^{1/4}$,

$$\frac{dn}{dt} = \frac{dn}{da}\frac{da}{dt} \propto n(a, t)\ a^{-3} \sim t^{(\alpha-3)/4}. \tag{8}$$

This is a well-known result for the delay-time distribution of the gravitational-wave-induced mergers of a single-age population, having an initial separation distribution that is a power law of index α (e.g. Greggio 2005; Totani et al. 2008).

Let us consider now a series of binary WD populations, each with an initial separation distribution $n'(a') \propto a'^{\alpha}$, being produced at a rate $R(t)$ between $t = 0$ and the present age of the Galaxy, t_0. The present-day distribution will be

$$N(a) = \int_0^{t_0} R(t_0 - t)n(a, t)dt \tag{9}$$

$$\propto \int_0^{t_0} R(t_0 - t)a^3(a^4 + Kt)^{(\alpha-3)/4}dt.$$

Assuming, for instance, a constant star-formation rate over the age of the Galaxy, then also $R(t) = \text{const}$. (Even if the star-formation history is "bumpy", the WD formation history will be the convolution of the star-formation history with a broad, $\sim t^{-0.5}$, kernel, that describes the WD supply [e.g., Pritchet et al. 2008], and which will smooth out the WD production rate). The integral then gives

$$N(x) \propto x^{4+\alpha}[(1 + x^{-4})^{(\alpha+1)/4} - 1], \qquad \alpha \neq -1, \tag{10}$$

or

$$N(x) \propto x^3 \ln(1 + x^{-4}), \qquad \alpha = -1, \tag{11}$$

where

$$x \equiv \frac{a}{(Kt_0)^{1/4}} \tag{12}$$

is the separation in units of the separation of binaries that will merge within the age of the Galaxy. For example, for $t_0 = 10$ Gyr and $m_1 = m_2 = 0.55$ $M_\odot$, $x = 1$ corresponds to $a_0 = 0.01$ AU, or 1.5×10^6 km, or about 150 WD radii. The right panel on Figure 3 shows $N(x)$ for various values of α. $N(x)$ is, again, approximately a broken power law, with index α at $x \gg 1$. At $x \ll 1$ the power-law index is 3 for $\alpha \geq -1$, and $\alpha + 4$ for $\alpha \leq -1$.

2.4.2. *Choice of binary separation*

We use the functional forms in Eqns. 10-11 to model the possible present-day distributions of DD separations, for various indices α of the initial power-law distributions at formation. In realizations of our simulation, we draw the separation of specific component binary masses from the present-day distribution for a particular value of α, with a between $a_{\min} = 2 \times 10^4$ km (contact) and $a_{\max} = 0.05$ AU. For the purpose of producing simulated radial velocities, binaries with periods < 15 min are assigned zero orbital velocity, as the SDSS exposure length prevents detection of velocity differences in such cases. A practical consideration in this process is the large dynamic range that the distribution $P(a)$ can assume over this range in a. As a result, very few simulated binaries might be assigned separations in ranges that have low probability, and the model expectation values for the the velocity differences due to those binaries will have large Poisson errors. To avoid this, we populate the distribution evenly with simulated systems among four decades of separation a (i.e., from $a_{\min}$ to $a_{\max}/1000$, from $a_{\max}/1000$ to $a_{\max}/100$, etc.). Each binary system is given a relative weight according to the integral of the separation distribution over the decade it is in.

2.5. *Period, orbital velocities, and merger rates*

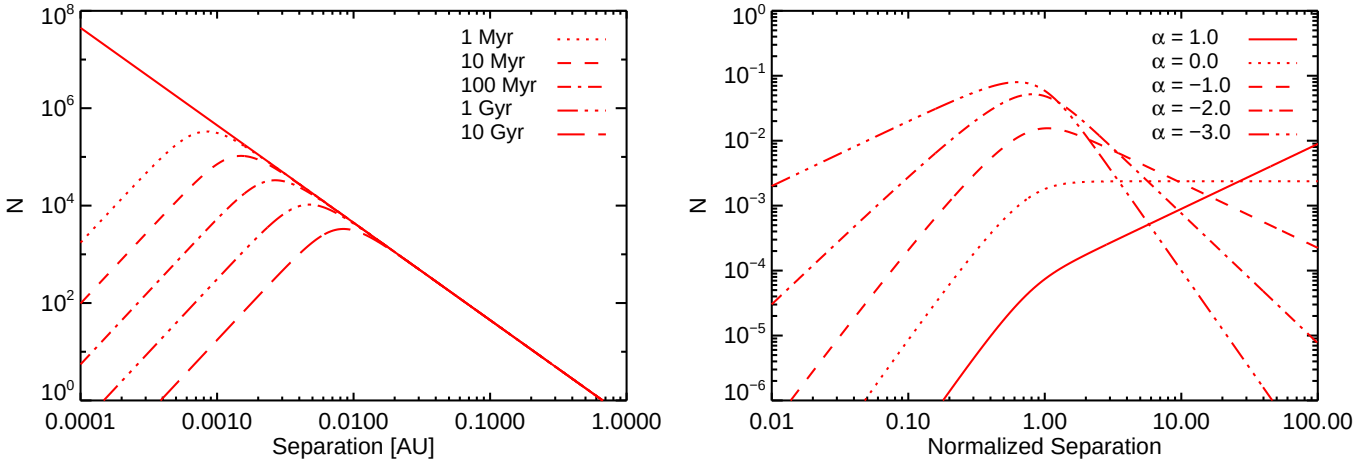

FIG. 3.— *Left*: Example of the gravitational-wave-driven time evolution of the separation distribution of a population with an initial power-law separation distribution of index $\alpha = -2.0$ (Eq. 7). In this example, both WDs are of 0.55 $M_\odot$. *Right*: Separation distributions for various values of α, time-integrated over a constant star-formation rate over 10 Gyr in the Galactic disk (Eqns. 10-11). Separations are relative to the initial separation of two 0.55 $M_\odot$WDs that will merge within 10 Gyr, $a = 0.01$ AU.

Given two masses and an orbital separation, Kepler's law gives the period

$$\tau = 2\pi \left(\frac{a^3}{G(m_1 + m_2)} \right)^{1/2}, \qquad (13)$$

and the circular orbital velocities,

$$v_1 = \frac{2\pi a}{\tau} \frac{m_2}{m_1 + m_2}, \quad v_2 = \frac{2\pi a}{\tau} \frac{m_1}{m_1 + m_2}. \qquad (14)$$

We assume circular velocities for simplicity, but also because this is the expectation for close binaries that have likely undergone circularization by tidal forces and common-envelope evolution. For example, there are essentialy no binaries with $P < 12$ d that have any appreciable eccentricity (Raghavan et al. 2010). It has been recently suggested (Thompson 2010) that there might be a preponderance of triple systems among binary WDs that would induce elliptical orbits via the Kozai (1962) mechanism, leading to a large population of systems with short merger times. We defer the exploration of this scenario to future work. Equation 3 with $a = 0$ gives the merger time, $t_{\rm merge}$, of the simulated system. The merger rate per WD in the simulated sample is obtained by noting, for a given set of parameters, the fraction of all of the systems in the simulation that merge within a set time window, divided by that time. Each system is weighted according to its decade in separation (see section 2.4.2, above). A separate tally is conducted to calculate the merger rate of only those binaries whose summed masses exceed the Chandrasekhar mass, which may be of relevance for the type-Ia supernova rate. For $\alpha \geq -1$, the merger rate is approximately constant, and therefore the time window for numerically calculating the rate is arbitrary, as long as it is shorter than t_0. The constancy of the rate can be seen from Eq. 10, by noting that mergers come from systems with $x < 1$, for which $N(x) \sim x^3$, and the merger rate is

$$\frac{dN}{dt} = \frac{dN}{da}\frac{da}{dt} \propto N(a)\ a^{-3} \sim {\rm const.} \qquad (15)$$

For $\alpha < -1$, the merger rate falls with time, but quite slowly for values of α that are not too steep,

$$\frac{dN}{dt} \sim N(a)\ a^{-3} \sim a^{\alpha+1} \sim t^{(\alpha+1)/4}, \qquad (16)$$

so an accurate numerical merger rate is still obtained in the above scheme.

The merger rate for a given combination of $f_{\rm bin}$ and α can also be roughly estimated analytically. If $\alpha \geq -1$, the majority of pairs have large separations, with long times until merger. The merger rate is therefore set by the integrated effect of old systems. All binaries with separations of $a < a_0$ at their formation time will contribute (at a constant rate, as we saw) to the current merger rate, where a_0 is the maximum separation binary that merges within t_0. Every choice of component masses gives a different value of a_0. However, for the range of possible component masses, a_0 is between 0.005 and 0.018 AU and a value of $a_0 = 0.01$ AU is typical. The typical time until merger of each system is t_0. The merger rate per observed WD is therefore

$$\frac{1}{N_{\rm wd}}\frac{dN}{dt} \approx \frac{f_{\rm bin}}{(1-f_{\rm bin})t_0} \frac{\int_{a_{\rm min}}^{a_0} n(a)da}{\int_{a_{\rm min}}^{a_{\rm max}} n(a)da} \qquad (17)$$

$$= \frac{f_{\rm bin}}{(1-f_{\rm bin})t_0} \frac{(a_0/a_{\rm min})^{\alpha+1} - 1}{(a_{\rm max}/a_{\rm min})^{\alpha+1} - 1},$$

for $n(a) = a^\alpha$. If $f_{\rm bin}$ is small, and (as in the present case), $a_{\rm max}$ and a_0 are both much larger than $a_{\rm min}$, then the merger rate is roughly

$$\frac{1}{N_{\rm wd}}\frac{dN}{dt} \approx \frac{f_{\rm bin}}{t_0} \left(\frac{a_0}{a_{\rm max}} \right)^{\alpha+1}. \qquad (18)$$

This gives values in good agreement with the merger rates from the numerical Monte Carlo calculation. One can also see from Eq. 18 that, in a plot of the parameter space of α vs. $\log f_{\rm bin}$, curves of constant merger rate will be straight lines with slope of $1/\log(a_0/a_{\rm max}) \approx 1.4$, for $a_0 = 0.01$ AU and $a_{\rm max} = 0.05$ AU (see Paper II). For $\alpha \ll -1$, most WD binaries are formed with small separations and therefore merge within a time much shorter than t_0. In this case, the merger rate will be controlled

by the supply rate of new WDs, which in turn is set by the star-formation rate.

2.6. *Inclination, photometric primary, temporal sampling, and velocity error*

We next apply observational effects to each simulated binary sytem. First, a line-of-sight inclination i of the perpendicular to the orbital plane is chosen from a distribution

$$P(i) \propto \sin i, \tag{19}$$

and the line-of-sight velocity is reduced by $\sin i$.

We then need to decide which of the two WDs will be the photometric primary. This could be either the less massive WD, because it has larger surface area and/or it is younger and hence hotter; or the more massive WD, because it cools more slowly due to its small surface area and is hence hotter. In practice, these effects compete against each other, and it is difficult to determine which of the two components will dominate the spectral energy distribution. From an observational point of view, the distribution of absolute magnitudes as a function of WD mass in the DR7 SDSS catalog shows a large spread about the mean at all masses, although low mass WDs (below $\sim$0.35 $M_\odot$) do seem to be intrinsically brighter (see Figure 4). From a theoretical point of view, the cooling curves of Fontaine et al. (2001) also predict that, in coeval DD systems, WDs with masses below ~ 0.35 $M_\odot$ will remain substantially brighter than their more massive counterparts for several hundred Myr (in the SDSS g filter – the effect is enhanced in r, and diminished in u). After about 1 Gyr, the slower cooling of more massive WDs takes over and makes them brighter, but by this time the predicted magnitudes become fainter than the cutoff in our samples for most of the volume probed by SDSS. To summarize, it seems reasonable to assume that low-mass WDs, if present, will have a tendency to dominate the spectral energy distribution of DD systems, but in other cases either of the components may be dominant. In our Monte Carlo runs, we therefore make the less massive WD the photometric primary when its mass is below 0.35 $M_\odot$, but decide randomly between the two WDs when the less massive WD is above this limit.

Once the photometric primary has been selected, we sample its line-of-sight velocity with the actual distribution of temporal samplings in the SDSS data. We do this by choosing at random a particular observation pattern (number of epochs and time between epochs) from the sample, with a random phase assigned to the first epoch of the sinusoidal RV curve. Figure 5 shows the distributions of the number of epochs and of the temporal baselines per object for the SDSS sample of Paper II. To each simulated velocity measurement, we add a random error that we draw from a Gaussian distribution, with the variance of the Gaussian drawn from the actual distribution of measurement errors for the observed sample (see figure 1 in Paper II for this distribution for the SDSS sample). Finally, for every simulated system or non-binary WD, we find the minimum and maximum observed velocities and calculate ΔRV_{max}.

For every parameter combination that defines a binary WD population model, we produce 10^5 WD systems (either single or binary, according to f_{bin}), and find the fractional prediction for each bin in the model ΔRV_{max} distribution. Multiplied by the observed WD sample size, this gives the expectation value for that bin.

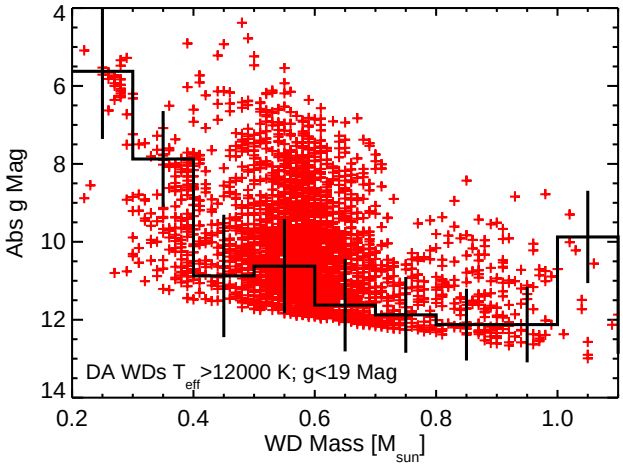

FIG. 4.— Distribution of absolute g magnitudes as a function of mass for the hot DA WDs in the DR7 catalog. We only consider, in this figure, objects with $T_{\rm eff}$ above 12000 K and g mag brighter than 19, for which spectroscopic masses can be modeled reliably. The overlaid histogram shows the mode (most frequent g magnitude observed) and the standard deviation in bins of 0.1 $M_\odot$. There is a large spread in absolute magnitudes at all masses, but low mass WDs (below $\sim$ 0.35 $M_\odot$) do seem to be intrinsically brighter.

3. RESULTS

Figure 6 shows the simulated ΔRV_{max} distribution for a model binary population with a particular set of parameters (f_{bin}, α, β), when a sample of that population is sampled with a particular set of empirical temporal sequences and a particular velocity error distribution. The observational parameters chosen are those of the SDSS sample presented in Paper II, and the model parameters are one set among those that reproduce the data. Along with this distribution, we plot the predictions for a model with *no* binaries in it. We see that the modeled ΔRV_{max} distribution consists of two parts. At low ΔRV_{max}, there is a "core" that is dominated by random velocity errors, that have been applied to systems that are single, or that have low ΔRV_{max} because of one or more causes (low orbital velocity, low inclination, inopportune sampling). Beyond this core, the distribution has a "tail" that reveals those close binaries that happened to have large orbital velocities, favorable inclinations, and temporal sampling that caught their velocity variations. For any observational sample, one can always calculate this zero-binaries core. When compared to the observed ΔRV_{max} distribution, it immediately reveals if and where in the data there exists a tail of real binary systems. A statistical comparison between the data and a grid of model distributions can then select the regions of binary population parameter space that are allowed or ruled out by the data.

A reliable estimate of the RV errors is essential, as otherwise underestimated errors can masquerade as a tail, or overestimated errors can hide a real binary population. This is also illustrated in Fig. 6, where we show several no-binary predictions that use incorrect error distributions, i.e., error distributions that are different from the one used to generate the distribution with binaries.

The temporal sampling density of the survey will naturally affect both the core and the tail of the ΔRV_{max}

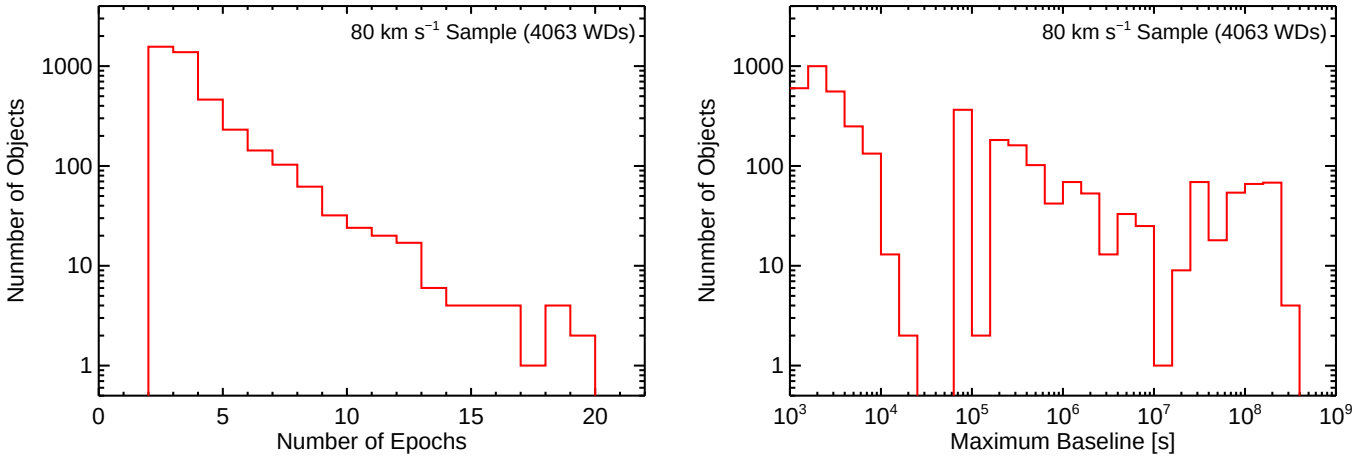

FIG. 5.— Temporal sampling characteristics for the DR7 WD sample analyzed in Paper II, and used in the example simulations here. *Left:* Distribution on number of epochs per object. Most WDs have only two or three epochs, but there is a tail of objects with more epochs. *Right:* Distribution of maximum time differences between epochs. A 45 min interval is most common, but longer timescales, of order an hour or of several days, are probed in many cases.

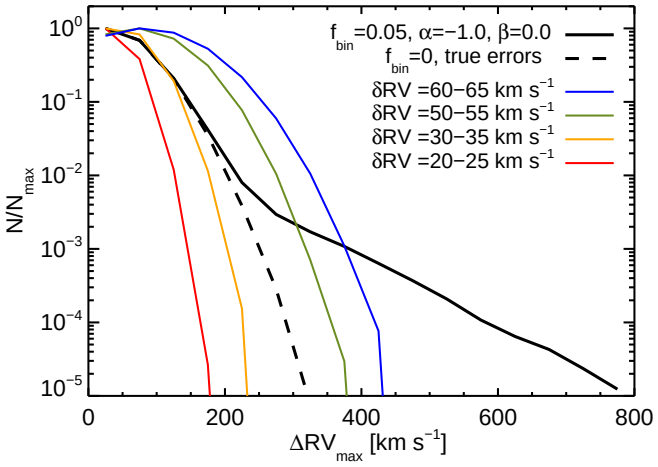

FIG. 6.— Simulated distributions of $\Delta\mathrm{RV}_{\max}$. Solid line shows the distribution resulting for a WD population with binary fraction $f_{\rm bin}$=0.05, separation distribution power-law index $\alpha = -1$, and mass-ratio distribution power-law index $\beta = 0$, when this distribution is observed with the temporal sequences and RV errors of the DR7 sample presented in Paper II. The dashed line shows the "core" of the distribution, obtained by setting $f_{\rm bin}$=0 (no binaries, except for the extremely low-mass WDs, which are always in binaries), and reflects the part of the full distribution that is due to RV errors alone. Colored curves show the core distributions obtained when assuming incorrect error distributions (various narrow distributions of 1σ error ranges, as marked). Accurate characterization of the errors is thus essential for characterizing the binary population by means of the signal in the tail of the $\Delta\mathrm{RV}_{\max}$ distribution.

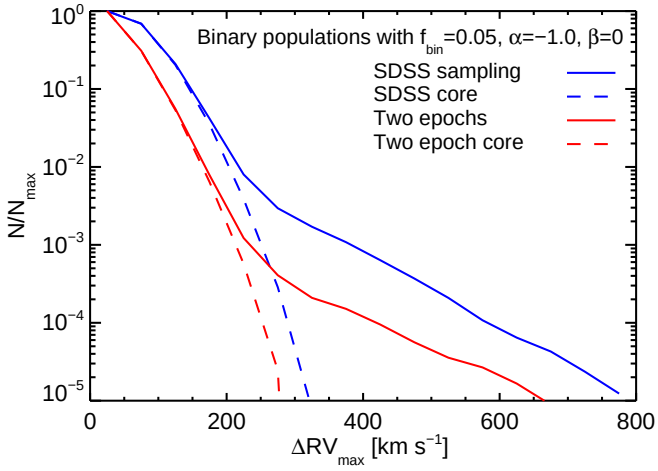

FIG. 7.— Dependence of $\Delta\mathrm{RV}_{\max}$ distribution on temporal sampling. Blue curves show the full $\Delta\mathrm{RV}_{\max}$ distribution (solid curves) and the $f_{\rm bin}$=0 core (dashed curve), for a chosen set of binary population parameters, and with the actual DR7 Paper II sample with its temporal sampling characteristics (same as Fig. 6.) Red curves show the distribution and core when every object is observed on two epochs only.

distribution. The more epochs per object, the greater the chance of catching the full RV variation range of each system. The core will also grow, but only as the square root of the number of epochs. Since the fully revealed RV range reaches saturation beyond some number of epochs, while the core $\Delta\mathrm{RV}_{\max}$ continues to grow as random errors are added in quadrature, there will be a limiting typical number of epochs, N, beyond which the technique is no longer efficient for characterizing the population, and one can, instead, attempt to fit RV curves to each object. This will happen when $\sqrt{N}\sigma_v \sim \Delta\mathrm{RV}_{\max+}$, where the latter is the highest value of $\Delta\mathrm{RV}_{\max}$ for which a sample has some exemplars, and σ_v is the typical velocity error. Fig 7 illustrates how the core and the tail of the distribution change when, instead of the full sampling of the SDSS dataset, every object is sampled only twice.

Figure 8 shows how the $\Delta\mathrm{RV}_{\max}$distribution depends on the binary population parameters $f_{\rm bin}$, α, and β. Qualitatively, increasing $f_{\rm bin}$ and decreasing α both have the same effect of increasing the number of small-separation binaries, and therefore of raising the high $\Delta\mathrm{RV}_{\max}$ tail of the distribution. Quantitatively, if we were dealing with a population of binaries with single values of component masses, single values of inclination angle, numerous sampling per object, and no measurement errors, then the $\Delta\mathrm{RV}_{\max}$ distribution tail would behave as

$$\frac{dN}{dv} = \frac{dN}{da}\frac{da}{dv}, \qquad (20)$$

and the broken power-law separation distribution, $N(a)$, would lead to a broken power-law orbital velocity distribution. Recalling that, for $\alpha > -1$, the small-separation part of the separation distribution behaves as $N(a) \propto a^3$, and taking the Keplerian $v \propto a^{-1/2}$, we would then ex-

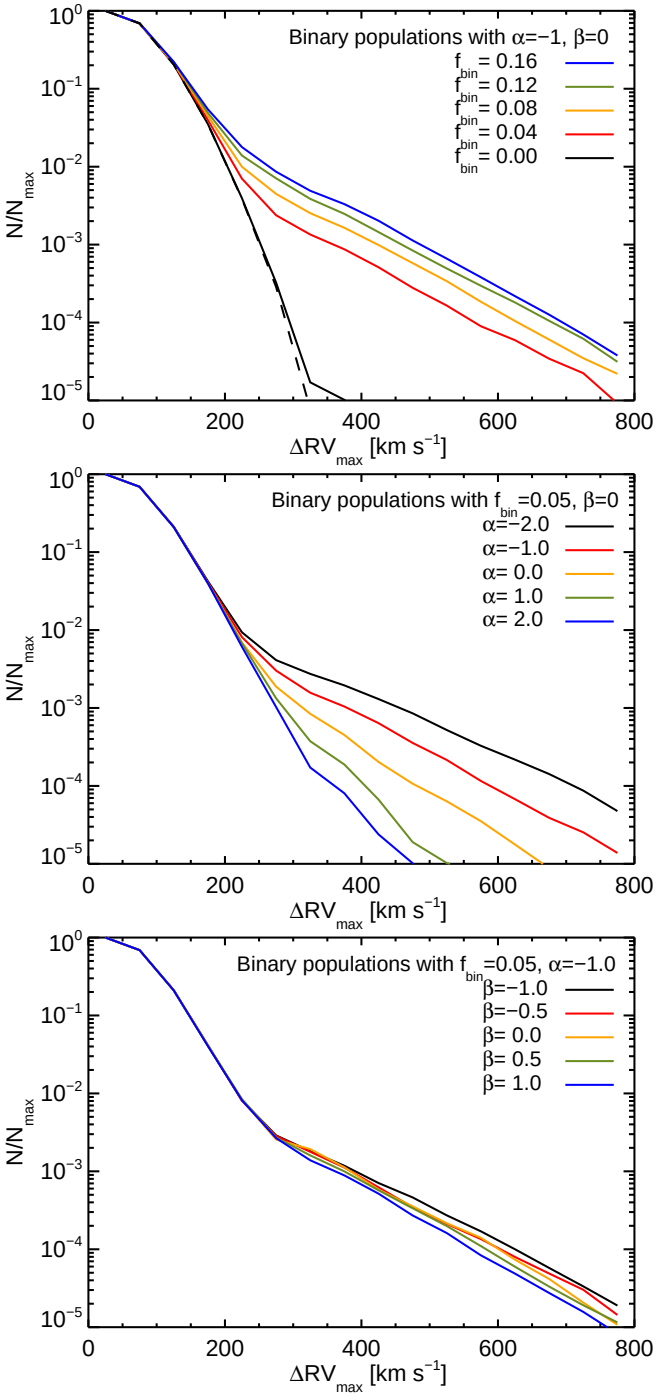

FIG. 8.— Dependence of the ΔRV_{max} distribution on binary population parameters. *Top:* Dependence of binary fraction, f_{bin}. The black solid curve is for no binaries, except for those that include a < 0.25 $M_\odot$WD. The dashed curve is with no binaries at all, and shows the bare "core" of the distribution, due to the radial velocity errors. *Middle:* Dependence on separation distribution power law index, α. *Bottom:* The weak dependence on the mass-ratio distribution's power-law index, β.

pect the tail to fall steeply as $\sim v^{-9}$ (for all $\alpha > -1$), with its amplitude depending on $f_{bin}/(\alpha+1)$ (the latter factor entering through the normalization of the distribution). The a^α branch of $N(a)$ at $a > a_0$ would transform to a $v^{-2\alpha-3}$ power law at velocities $v < v_0$, where v_0 is the orbital velocity of a binary with separation a_0. In reality, the distribution of component masses (which leads to a range of values for a_0), the projection of velocities due to inclination, and the sampling (both of which effects move binaries in the distribution to lower values of ΔRV_{max}), and the velocity errors (which again mix the distribution), will lead to a ΔRV_{max} tail with a slope that behaves differently than above, and does depend on α. For $\alpha < -1$, $N(a) \propto a^{\alpha+4}$, and the ΔRV_{max} distribution tail falls more gently, as $\sim v^{-2(\alpha+11)}$, in the idealized case. Thus, in principle, α can be discerned in data with low-enough velocity errors, and with large enough samples, such that the slope of the tail can be measured accurately.

As seen in Fig. 8, the ΔRV_{max} distribution is weakly dependent on β, the power-law index of the binary mass-ratio distribution. For a given choice of primary mass, the secondary's velocity will depend on the mass ratio q as $(1+q)^{-1/2}$. For the typical $m_1 \lesssim 0.75$ $M_\odot$ primary mass, the secondary mass is constrained to the range from m_1 down to $m_{lim} = 0.25$ $M_\odot$, so q is between about 1/3 and 1. Going from high positive values of β that favor q near 1, to very negative β's that concentrate q for all binaries to be near 1/3, will induce an increase of $\sqrt{3/2} = 1.22$ in the secondary's velocity v_2, and an even smaller relative decrease, by 0.93, in v_1, if it is the primary that is selected as the photometric primary. Thus when changing between the extreme values of β, about half of the binaries will have their ΔRV_{max} increase by 22%, and half will decrease by 7%, or a net increase by 7% in the ΔRV_{max} of each bin in the distribution. Even for the highest velocities that we consider, this is a small change, comparable to the typical velocity errors. Furthermore, as we saw above, the ΔRV_{max} distribution is roughly a power law. The transformation $v \rightarrow v' = kv$, where k is a constant, does not affect the shape of power-law distribution in v.

4. CONCLUSIONS

We have used Monte Carlo simulations to study how the distribution of maximal radial velocity differences, ΔRV_{max}, can characterize a close binary population, in a radial velocity survey where a large number of stars are observed, but with only a few epochs per star, and with potentially large RV errors. Our focus has been on a survey for double WDs of the kind that we analyze in Paper II, using the SDSS DR7 WD sample, which has served here as our example survey in terms of observational parameters. As part of this modeling process, we required a realistic representation of the present day separation distribution of close WD binaries whose separations have evolved due to gravitational wave emission. We have therefore derived analytical expressions for the separation distribution of a population of WD binaries that is continuously formed, its orbits decay, and some of its members merge, over the lifetime of the Galaxy. With these simulations, we have determined how the ΔRV_{max} distribution depends on the binary population, which we have characterized using three parameters (describing close-binary fraction, separation distribution, and mass-ratio distribution), and on the observational parameters of the sample – RV errors and temporal sampling pattern.

Our main findings are:

1. The ΔRV_{max} distribution has a core region, that

is produced by the random RV errors, and a tail, that can reveal the presence of some of the close binaries in a sample. The power of the technique is that, even with large errors and only few (or even just two) epochs per object, the close binary population can reveal itself in the tail, provided that the number of objects in the sample is large enough. This tail permits statistically constraining the properties of the population, even with sparse and noisy data, and without detailed followup work on candidate binary systems.

2. Accurate knowledge of the distribution of radial velocity errors is essential to model properly the $\Delta\mathrm{RV}_{\max}$ distribution, and thus deduce the contribution of the real binary population to the tail.

3. Steep distributions in initial separation (very negative α, with most binaries at small separations) and populations with a large close-binary fraction (large $f_{\rm bin}$) will both result in an increase in the amplitude of the $\Delta\mathrm{RV}_{\max}$ tail. There may thus be some degeneracy in the determination of these two parameters. A change in α, however, also changes the shape of the tail, and hence, in high-quality datasets (many objects, small errors), these parameters may still be individually constrained.

4. The $\Delta\mathrm{RV}_{\max}$ distribution depends weakly on the details of the distributions of the component binary WD masses – the distributions of primary masses and of secondary mass ratios, which in any case are chosen from a a relatively small dynamic range. This binary population characteristic thus cannot be constrained by this kind of survey data. Conversely, not knowing the distribution of mass ratios does not affect adversely our ability to constrain the other binary population parameters.

5. The $\Delta\mathrm{RV}_{\max}$ approach allows to estimate the merger rate of a close binary population, based on noisy RV data with few epochs, of the kind we consider. This is possible without follow-up observations to obtain full binary parameter solutions for candidates, and without necessarily even finding a single binary that will merge within a Hubble time. This ability is a result of the statistical nature of our approach.

In Paper II we apply the methods presented here to the observed SDSS DR7 WD sample, we set constraints on the local population parameters of close-WD binaries in the Galaxy, and we derive the merger rate of this population, both in general and for particular component and total mass ranges. We show that the local rate of WD mergers with super-Chandrasekhar total masses is an order of magnitude lower than the local Type-Ia supernova rate. The local merger rate of all WDs, however, is remarkably similar to the Type-Ia suparnova rate. A large fraction of all WD mergers are between CO and CO WDs, with total masses not far from the Chandrasekhar limit. If sub-Chandrasekhar mergers result in a Type-Ia supernova explosion, we may have identified their dominant progenitors.

Apart from Type-Ia supernova explosions, other possible outcomes of WD mergers can be tested with our methodology – R Corona Borealis stars (e.g. Longland et al. 2011), or highly magnetic WDs, which have been postulated to result from WD mergers (e.g. García–Berro et al. 2012, and references therein). Some $7 \pm 3\%$ of local WDs have magnetic fields greater than 10^7 G (Kawka et al. 2007). Assuming these magnetic fields decay on very long timescales, WD mergers producing all of this population would need to occur, over 10 Gyr, the age of the Galaxy, at a rate of $\sim (7 \pm 3) \times 10^{-12}$ yr^{-1} per WD. In Paper II, our fit to the observed $\Delta\mathrm{RV}_{\max}$ distribution for the WDs in SDSS indicates a WD merger rate, for total merged masses of < 1 M$_\odot$, of $1^{+3}_{-0.7} \times 10^{-12}$ yr^{-1} per WD. The rate may thus be sufficient to explain at least some, and perhaps even all, magnetic WDs with such mergers.

As another example, about half of WDs with masses below 0.45 M$_\odot$ appear to be single (Maxted et al. 2000; Napiwotzki et al. 2007; Kilic et al. 2007). Nelemans & Tauris (1998) have suggested formation of such low-mass single WDs via interaction between a giant star and a close massive-planet or brown-dwarf companion, followed by evaporation or tidal disruption of the companion. Kilic et al. (2007) have proposed that these WDs have evolved from metal-rich stars whose evolution was truncated by severe mass loss on the giant branch. Alternatively, Iben et al. (1997) have raised the possibility that the single low-mass WDs are the merger products of even-lower WDs. Our constraints on merger rates can test this last scenario. In the Kepler et al. (2007) WD mass function, about 8% of the WDs are in a Gaussian component that peaks at around 0.4 M$_\odot$. Assuming that half of these WDs are single, then in the Iben et al. (1997) scenario, about 4% of the WD population would be the outcome of very-low-mass WD mergers. This is a similar fraction to the one invoked above in the case of magnetic WDs, and therefore would require a similar merger rate. Our calculations, however, show that the rate of mergers with total masses in the range 0.3–0.5 M$_\odot$ is four orders of magnitude below the one required by this scenario. This comes about because each of the merging WDs would need to be below 0.3 M$_\odot$, and such WDs are rare. The longer gravitational orbit decay time at these low masses further lowers the rate. One could circumvent this argument by invoking large mass loss during the merger process (e.g. Fryer et al. 2010), so that more massive and common WDs could be involved. However, Dan et al. (2012) find negligible mass loss in their 3D hydrodynamic simulations of WD mergers.

The tools that we have introduced here can also easily be adapted to the characterization of stellar multiplicity based on large RV surveys in other settings. Examples are ongoing surveys like LAMOST (Su et al. 1998) and APOGEE (Prieto et al. 2008), and planned ones, such as BigBOSS (Schlegel et al. 2011).

We thank Scot Kleinman for making his DR7 WD catalog available to us in advance of publication. We acknowledge useful comments and suggestions from Tim Beers, Pierre Bergeron, Warren Brown, Joke Claeys, Brian Metzger, Gijs Nelemans, Marten van Kerk-

wijk, Lev Yungelson, and the anonymous referee. We are grateful to all members of the SWARMS team: Mukremin Kilic, Tom Matheson, Fergal Mullally, Tony Piro, Roger Romani, and Susan Thompson. DM acknowledges support by a grant from the Israel Science Foundation.

Funding for the SDSS and SDSS-II has been provided by the Alfred P. Sloan Foundation, the Participating Institutions, the National Science Foundation, the U.S. Department of Energy, the National Aeronautics and Space Administration, the Japanese Monbukagakusho, the Max Planck Society, and the Higher Education Funding Council for England. The SDSS Web Site is http://www.sdss.org/. The SDSS is managed by the Astrophysical Research Consortium for the Participating Institutions. The Participating Institutions are the American Museum of Natural History, Astrophysical Institute Potsdam, University of Basel, University of Cambridge, Case Western Reserve University, University of Chicago, Drexel University, Fermilab, the Institute for Advanced Study, the Japan Participation Group, Johns Hopkins University, the Joint Institute for Nuclear Astrophysics, the Kavli Institute for Particle Astrophysics and Cosmology, the Korean Scientist Group, the Chinese Academy of Sciences (LAMOST), Los Alamos National Laboratory, the Max-Planck-Institute for Astronomy (MPIA), the Max-Planck-Institute for Astrophysics (MPA), New Mexico State University, Ohio State University, University of Pittsburgh, University of Portsmouth, Princeton University, the United States Naval Observatory, and the University of Washington.

REFERENCES

Badenes, C. & Maoz, D. 2012 ApJL, submitted [Paper II]
Belczynski, K. & Taam, R. E. 2004, ApJ, 616, 1159
Bressert, E., Bastian, N., Gutermuth, R., Megeath, S. T., Allen, L., Evans II, N. J., Rebull, L. M., Hatchell, J., Johnstone, D., Bourke, T. L., Cieza, L. A., Harvey, P. M., Merin, B., Ray, T. P., & Tothill, N. F. H. 2010, MNRAS, 409, L54
Brown, W. R., Kilic, M., Allende Prieto, C., & Kenyon, S. J. 2012, ApJ 744, 142
Bruzual, A. G. & Charlot, S. 1993, ApJ, 405, 538
Claeys, J. S. W., Pols, O. R., Vink, J., & Izzard, R. G. 2011, eprint arXiv:1101.5601
Clark, B. M., Blake, C. H., & Knapp, G. R. 2011, eprint arXiv:1110.4016
Conroy, C., Gunn, J. E., & White, M. 2009, ApJ, 699, 486
Dan, M., Rosswog, S., Guillochon, J., & Ramirez-Ruiz, E. 2012, arXiv:1201.2406
Deloye, C. J. & Taam, R. E. 2010, ApJ, 719, L28
Duquennoy, A. & Mayor, M. 1991, A&A, 248, 485
Fontaine, G., Brassard, P., & Bergeron, P. 2001, PASP, 113, 409
Fryer, C. L., Ruiter, A. J., Belczynski, K., et al. 2010, ApJ, 725, 296
García–Berro, E., Lorén–Aguilar, P., Aznar–Siguán, G., et al. 2012, arXiv:1202.0461
Goodwin, S. P. & Kroupa, P. 2005, A&A, 439, 565
Greggio, L. 2005, A&A, 441, 1055
Iben, I., Jr., Tutukov, A. V., & Yungelson, L. R. 1997, ApJ, 475, 291
Ivanova, N. 2011, in ASP Conference Proceedings, Vol. 447 (San Francisco, CA:ASP), 91
Izzard, R. G., Dray, L. M., Karakas, A. I., Lugaro, M., & Tout, C. A. 2006, A&A 460, 565
Kawka, A., Vennes, S., Schmidt, G. D., Wickramasinghe, D. T., & Koch, R. 2007, ApJ, 654, 499
Kepler, S. O., Kleinman, S. J., Nitta, A., Koester, D., Castanheira, B. G., Giovannini, O., Costa, A. F. M., & Althaus, L. 2007, MNRAS, 375, 1315
Kilic, M., Stanek, K. Z., & Pinsonneault, M. H. 2007, ApJ, 671, 761
Kleinman, S. J., Nitta, A., & Koester, D. 2009, JoP: Conference Series, 172, 012020
Kozai, Y. 1962, ApJ, 67, 591
Longland, R., Lorén-Aguilar, P., José, J., et al. 2011, ApJL, 737, L34
Makarov, V. V. & Kaplan, G. H. 2005, AJ, 129, 2420
Maoz, D., & Mannucci, F. 2011, arXiv:1111.4492
Marks, M. & Kroupa, P. 2011, MNRAS, 417, 1702
Marks, M., Kroupa, P., & Oh, S. 2011, MNRAS, 417, 1684
Marsh, T. R., Dhillon, V. S., & Duck, S. R. 1995, MNRAS, 275, 828
Mason, B. D., Hartkopf, W. I., Gies, D. R., Henry, T. J., & Helsel, J. W. 2009, ApJ, 137, 3358
Maxted, P. F. L., Ferrario, L., Marsh, T. R., & Wickramasinghe, D. T. 2000, MNRAS, 315, L41
Maxted, P. F. L. & Jeffries, R. D. 2005, MNRAS, 362, L45
Mazeh, T., Simon, M., Prato, L., Markus, B., & Zucker, S. 2003, ApJ, 599, 1344
Mennekens, N., Vanbeveren, D., De Greve, J. P., & De Donder, E. 2010, A&A, 515, A89
Metchev, S. A. & Hillenbrand, L. A. 2009, ApJS, 181, 62
Napiwotzki, R., Karl, C. A., Nelemans, G., et al. 2007, 15th European Workshop on White Dwarfs, 372, 387
Nelemans, G., & Tauris, T. M. 1998, A&A, 335, L85
Peters, P. C. & Mathews, J. 1963, Phys. Rev., 131, 435
Prada Moroni, P. G. & Straniero, O. 2009, A&A, 507, 1575
Prieto, C. A., Majewski, S., Schiavon, R., Cunha, K., Frinchaboy, P., Holtzman, J., Johnston, K., Shetrone, M., Skrutskie, M., Smith, V., & Wilson, J. 2008, AN, 329, 1018
Pritchet, C. J., Howell, D. A. & Sullivan, M. 2008, ApJ, 683, L25
Raghavan, D., McAlister, H. A., Henry, T. J., Latham, D. W., Marcy, G. W., Mason, B. D., Gies, D. R., White, R. J., & ten Brummelaar, T. A. 2010, ApJS, 190, 1
Rebassa-Mansergas, A., Nebot Gómez-Morán, A., Schreiber, M. R., Girven, J., Gänsicke, B. T. 2011, MNRAS, 413, 1121
Ruiter, A. J., Belczynski, K., & Fryer, C. 2009, ApJ, 699, 2026
Schlegel, D., et al. 2011, eprint arXiv:1106.1706
Su, D. Q., Cui, X., Wang, Y., & Yao, Z. 1998, Proc. SPIE Vol. 3352, 3352, 76
Thompson, T. A. 2010, eprint arXiv:1011.4322
Tohline, J. E. 2002, ARA&A, 40, 349
Toonen, S., Nelemans, G., & Portegies Zwart, S. 2011, arXiv:1101.2787
Totani, T., Morokuma, T., Oda, T., Doi, M., & Yasuda, N. 2008, PASJ 60, 1327
Tutukov, A. V., & Yungelson, L. R. 1986, AZh, 63, 1012
Wang, B., Li, X.-D., & Han, Z.-W. 2010, MNRAS, 401, 2729
Williams, K. A., Bolte, M., & Koester, D. 2009, ApJ, 693, 355
Woods, T. E., Ivanova, N., van der Sluys, M. V., & Chaichenets, S. 2012, ApJ, 744, 12
York, D. G., et al. 2000, AJ, 120, 1579
Yungelson, L. R. 2010, Astronomy Letters, 36, 780